



HAL
open science

Aerosol characterization in an oceanic context around Reunion Island (AEROMARINE field campaign)

Faustine Mascout, Olivier Pujol, Bert Verreyken, Raphaël Peroni, Jean Marc Metzger, Luc Blarel, Thierry Podvin, Philippe Goloub, Karine Sellegri, Troy Thornberry, et al.

► **To cite this version:**

Faustine Mascout, Olivier Pujol, Bert Verreyken, Raphaël Peroni, Jean Marc Metzger, et al.. Aerosol characterization in an oceanic context around Reunion Island (AEROMARINE field campaign). Atmospheric Environment, 2022, 268, pp.118770. 10.1016/j.atmosenv.2021.118770 . hal-03815612

HAL Id: hal-03815612

<https://cnrs.hal.science/hal-03815612v1>

Submitted on 14 Oct 2022

HAL is a multi-disciplinary open access archive for the deposit and dissemination of scientific research documents, whether they are published or not. The documents may come from teaching and research institutions in France or abroad, or from public or private research centers.

L'archive ouverte pluridisciplinaire **HAL**, est destinée au dépôt et à la diffusion de documents scientifiques de niveau recherche, publiés ou non, émanant des établissements d'enseignement et de recherche français ou étrangers, des laboratoires publics ou privés.



Distributed under a Creative Commons Attribution - NonCommercial - NoDerivatives 4.0 International License

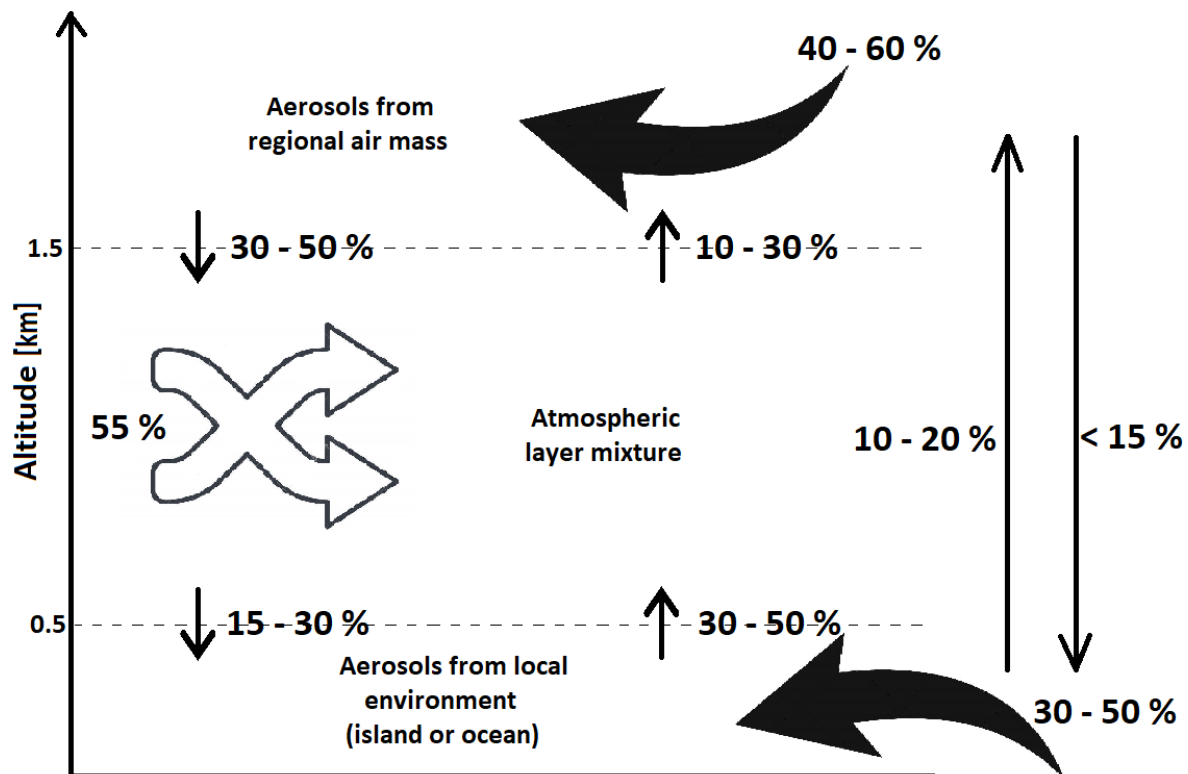
[Click here to view linked References](#)

1 Graphical Abstract

2 **Aerosol characterization in an oceanic context around Reunion Island (AEROMARINE field cam-**
3 **paign)**

4 Faustine Mascaut, Olivier Pujol, Bert Verreyken, Raphaël Peroni, Jean Marc Metzger, Luc Blarel, Thierry Podvin, Philippe Goloub, Karine

5 Sellegri, Troy Thornberry, Valentin Dufлот, Pierre Tulet, Jérôme Brioude



6 Highlights

7 **Aerosol characterization in an oceanic context around Reunion Island (AEROMARINE field cam-** 8 **paign)**

9 Faustine Mascout,Olivier Pujol,Bert Verreyken,Raphaël Peroni,Jean Marc Metzger,Luc Blarel,Thierry Podvin,Philippe Goloub,Karine
10 Sellegri,Troy Thornberry,Valentin Dufлот,Pierre Tulet,Jérôme Brioude

- 11 • Optical properties, vertical distribution and transport pathways, from the marine boundary layer to the free troposphere,
12 of marine aerosols in a pristine environment are examined.
- 13 • Aerosol size does not exceed the accumulation mode.
- 14 • A sketch is proposed as a characterization of marine aerosols distribution. Oceanic and insular influences in the aerosol
15 content are separated.
- 16 • It is argued that the AERONET station at St Denis (Reunion Island) is well representative of marine conditions.
- 17 • With the thermodynamics given by a microwave radiometer, the results will be useful for water vapor-aerosol-cloud
18 physical processes modeling in a pristine ocean.

Aerosol characterization in an oceanic context around Reunion Island (AEROMARINE field campaign)

Faustine Mascout^a, Olivier Pujol^{a,*}, Bert Verreyken^{b,c,d}, Raphaël Peroni^a, Jean Marc Metzger^e, Luc Blarel^a, Thierry Podvin^a, Philippe Goloub^a, Karine Sellegri^f, Troy Thornberry^{g,h}, Valentin Duflot^b, Pierre Tuletⁱ and Jérôme Brioude^b

^aUniversité de Lille, Département de Physique, Laboratoire d'Optique Atmosphérique (LOA), 59655, Villeneuve d'Ascq, France

^bLaboratoire de l'Atmosphère et des Cyclones (LACy), UMR 8105, Météo France/CNRS/Université de La Réunion, St Denis de La Réunion, France

^cRoyal Belgian Institute for Space Aeronomy, 1180 Brussels, Belgium

^dDepartment of Chemistry, Ghent University, 9000 Ghent, Belgium

^eObservatoire des Sciences de l'Univers de La Réunion, UMS3365, 97744 St Denis, France

^fLaboratoire de Météorologie Physique, Observatoire de Physique du Globe de Clermont-Ferrand, Université Blaise Pascal – CNRS, 63177 Aubière, France

^gNOAA Chemical Sciences Laboratory (CSL), Boulder, USA

^hCIRES, University of Colorado Boulder, Boulder, USA

ⁱLaboratoire d'Aérodynamique, Université de Toulouse, UT3, CNRS, IRD, 31400 Toulouse, France

ARTICLE INFO

Keywords:

Sea Salt Aerosols

Pristine conditions


Southern Indian Ocean

AEROMARINE field campaign

ABSTRACT

This article presents the results of the AEROMARINE field campaign which took place between February and April 2019 off the coast of Reunion Island in the South West Indian Ocean basin. The Southern Indian Ocean is of major interest for the study of marine aerosols, their distribution and variability. Six instrumented light plane flights and a ground-based microwave radiometer were used during the field campaign. These measurements were compared with the long-term measurements of the AERONET sun-photometer (based in St Denis, Reunion Island) and various instruments of the high altitude Maïdo Observatory (2.2 km above sea level, Reunion Island). These results were also analyzed using different model outputs: (i) the AROME mesoscale weather forecast model to work on the thermodynamics of the boundary layer, (ii) the FLEXPART-AROME Lagrangian particle dispersion model to assess the geographical and vertical origin of air masses, and (iii) the chemical transport model CAMS (Copernicus Atmosphere Monitoring Service) to work on the aerosol chemical composition of air masses. This allowed to highlight two points: (1) the atmospheric layer above 1.5 km is mainly composed of aerosols from the regional background; (2) the local environment (ocean or island) has little impact on the measured concentrations. Marine aerosols emitted locally are mostly measured below 0.5 km. The daytime marine aerosol distributions in the free troposphere measured by the aircraft were compared to the aerosol distribution measured at the high altitude Maïdo Observatory at night when the Observatory is located in the free troposphere. The results indicate that the high altitude site measurements are representative of the concentration of marine aerosols in the free troposphere. We also found that the CAMS reanalyses overestimated the aerosol optical depth in this region. Finally, our study strongly suggests that the AERONET station in St Denis (Reunion Island) can be considered as a representative marine station under the Tropics.

*Corresponding author

 faustine.mascaut@univ-lille.fr (F. Mascout);

olivier.pujol@univ-lille.fr (O. Pujol); bert.verreyken@aeronomie.be (B.

Verreyken); raphael.peroni@univ-lille.fr (R. Peroni);

jean-marc.metzger@univ-reunion.fr (J.M. Metzger);

luc.blarel@univ-lille.fr (L. Blarel); thierry.podvin@univ-lille.fr (T.

Podvin); philippe.goloub@univ-lille.fr (P. Goloub);

K.Sellegri@opgc.univ-bpclermont.fr (K. Sellegri);

troy.thornberry@noaa.gov (T. Thornberry);

19 1. Introduction

20 Because of their direct and indirect radiative forcings,

21 atmospheric aerosols have a major impact on the climate.

22 These forcings are still poorly understood and lead to uncer-

valentin.duflot@univ-reunion.fr (V. Duflot);

pierre.tulet@aero.obs-mip.fr (P. Tulet); jerome.brioude@univ-reunion.fr

(J. Brioude)

ORCID(s):

23 tainties that have persisted in models since the 1990s (Myhre 52 a region with frequent pristine conditions (where land and
 24 et al., 2013). One of the largest uncertainties of the aerosol- 53 human activities have little impact) that can reasonably be
 25 cloud system is the background concentration of natural aerosols, considered to be close to the preindustrial conditions. Few
 26 especially over clean marine regions (Andreae and Rosen- 55 data have been collected in this region (Pant et al., 2009).
 27 feld, 2008). Oceans cover about 70% of the Earth's surface 56 However, it is a crucial reference point to quantify the back-
 28 and are an important reservoir of marine aerosols (mainly 57 ground concentration of natural aerosols and the contribu-
 29 sea salt and organic aerosols). Sea Salt Aerosols (SSA) are 58 tion of natural emissions to the changing climate. In pristine
 30 one of the largest contributors to global aerosol loading and 59 regions, SSA are dominant and concentrations are relatively
 31 therefore they play an important role in global climate. Also, 60 low (*e.g.* Mallet et al., 2018).
 32 they were proposed to be a major component of primary 61 Reunion Island in the southwestern Indian Ocean can be
 33 marine aerosol mass over the regions where wind speeds 62 considered as a background aerosol pristine environment un-
 34 are high and/or other aerosol sources are weak (Gantt and 63 der trade wind conditions (Koren et al., 2014), mostly dur-
 35 Meskhidze, 2013; O'Dowd and de Leeuw, 2007). Luo et al. 64 ing the wet season from December to April. For details
 36 (2014) showed that the *AOD* at 532 nm of SSA in the Ma- 65 about wind circulation in the Southern Indian Ocean, includ-
 37 rine Boundary Layer (MBL) is governed by different physi- 66 ing Reunion Island, see the statistical study by Mallet et al.
 38 cal factors: the surface wind speed, Sea Surface Temperature 67 (2018) and refs therein. Reunion Island is also a unique site
 39 (SST), MBL height, lower troposphere stability, and relative 68 in the southern hemisphere for making aerosol observations.
 40 humidity (impact on size and optical properties of sea salt 69 Indeed, being in an oceanic environment and far from con-
 41 particles). However, there is a notable lack of data, in par- 70 tinent, the island is in a strategic location for carrying out
 42 ticular over the oceans and in the southern hemisphere, de- 71 measurements in a clean region, and also for the validation
 43 scribing the characteristics of aerosols such as optical prop- 72 of spatial measurements. In addition, the Maïdo Observa-
 44 erties, size distribution, temporal and spatial variabilities... 73 tory (located at 2.2 km above sea level (a.s.l)¹) allows: (i) to
 45 (Ramachandran, 2004). Pant et al. (2009) carried out mea- 74 take measurements directly in the free troposphere at night
 46 surements of the total number concentration and the size dis- 75 (Guilpart et al., 2017; Foucart et al., 2018) and (ii) to perform
 47 tribution of aerosols over the Indian Ocean in 2004. They 76 long-term *in-situ* observations including detailed profiles of
 48 observe that the aerosol concentration-wind speed correla- 77 wind, temperature and water, as well as concentration, size
 49 tion coefficient depends on the latitude and has a maximum 78 and chemical composition of aerosols collected by ground
 50 value where the winds are the strongest. 79 instruments (Baray et al., 2013).

¹In this paper, altitudes are given above sea level (a.s.l)

51 The southwestern Indian Ocean has been identified as

80 The AEROMARINE project, which took place between 109
 81 February and April 2019, aimed at collecting data on ma-110
 82 rine aerosol emissions, their optical properties, their trans-111
 83 port and distribution off the coast of the Reunion Island. For 112
 84 this, ground-based instruments and instruments on board ul-113
 85 tra light plane were used to measure concentration, size dis-114
 86 tribution and optical thickness of marine aerosols over the 115
 87 Indian Ocean, on the western side of Reunion Island. In ad-116
 88 dition, in order to characterize the thermodynamics of the 117
 89 MBL and the exchanges between the MBL and the free tro-118
 90 posphere, a MicroWave Radiometer Profiler (MWRP) was 119
 91 set up in St Denis (in the north of the island). Aerosol data
 92 have been complemented by the measurements of the AErosol¹²⁰
 93 RObotic NETwork (AERONET) sun-photometer (St Denis), 121
 94 and the various instruments of the Maïdo Observatory. Mod-122
 95 els, such as FLEXPART-MesoNH or AROME as well as 123
 96 Copernicus Atmosphere Monitoring Service (CAMS) reanal-124
 97 yses allowed to compare and/or support *in-situ* measurements. 125
 98 The instruments (on board and on the ground) and the mod-126
 99 els used are briefly presented in the following section. 127

100 The overall objectives of the AEROMARINE project in 128
 101 clude: 129

102 1) To characterize marine aerosol optical properties and 130
 103 their vertical distribution. The instruments on board the light 131
 104 plane helped characterize the marine aerosol optical proper-132
 105 ties, number concentration, and size distribution within the 133
 106 MBL and the free troposphere. Those results were compared 134
 107 with aerosol measurements at the Maïdo Observatory. Fur-135
 108 thermore, *AOD*-measurements were compared with those

of the AERONET station at St Denis.

2) To examine the transport pathways of marine aerosols from the boundary layer to the free troposphere. Hence, it is important to estimate accurately the vertical distribution of the marine aerosols. Indeed, the MBL dynamics affect marine emission mechanisms, vertical dilution, while shallow convection is important for exchange and mixing of aerosols with the free troposphere.

The aim of this paper is to present the results obtained (section 3) during AEROMARINE that answer the above objectives. Section 4 is the conclusion of this work.

2. Instruments and models used

2.1. On-board instruments

2.1.1. PLASMA

Photomètre Léger Aéroporté pour la Surveillance des Masses d'Air (PLASMA) is a sun-tracking photometer developed by LOA and SNO PHOTONS (Karol et al., 2013). Compact (23 cm) and light (3 kg), it can be put on different mobile platforms (Popovici et al., 2018). Sun tracking is performed by means of elevation (0 – 88 °) and azimuth (0 – 360 °) rotations. Aerosol Optical Depths (*AODs*) at various wavelengths² (λ) are derived from extinction measurements of the solar radiation by molecular and aerosol scattering and absorption processes. The instrument provides *AODs* over a wide spectral range ($\lambda = 0.34 - 2.25\mu\text{m}$) with an accuracy ΔAOD ranging from 0.005 to 0.01 according to λ . Aerosol size distribution is retrieved from the *AOD* spectral

²In this text, wavelengths are given with respect to the vacuum

dependence (Karol et al., 2013). The Angström exponent α which is indicative of grown nucleated particles, and fine
 is determined from the law of Angström: $AOD_1/AOD_2 = (\lambda_1/\lambda_2)^{-\alpha}$ marine primary aerosols (size range 50 – 100 nm) that dom-
 where AOD_i is the aerosol optical depth at the inate the primary marine aerosol size distribution (Schwier
 wavelength λ_i (Angström, 1961). This exponent describes et al., 2017).
 how the AOD varies with λ and so provides information on
 the size distribution of the aerosols (Kusmierczyk-Michulec
 et al., 2002).

2.1.2. Particle counters

The Portable Optical Particle Counter (POPS) is a 900 g *in situ* instrument designed by US laboratories NOAA and CIRES that provides aerosol number size distribution (in the size range 132 nm – 3 μ m) using single-particle light scattering (Gao et al., 2016). POPS is a prototype made by a 3D printer to reduce weight. It flew on board a light plane during the AEROMARINE intensive field campaign within the MBL and the free troposphere.

Two Condensable Particle Counters (CPCs) (accuracy: $\pm 20\%$) are used simultaneously to measure the total concentration of particles larger than 2 nm (CPC-MAGIC200) and particles larger than 10 nm (CPC TSI model 3007). The difference of concentration between the two CPCs gives the particle concentration in the size range 2 – 10 nm, which is indicative of the recent formation of nanometric particle, i.e. nucleation. The combination of two CPCs to investigate nucleation was proven to be adequate in past airborne studies (Crumevolle et al., 2010). Additionally, in synergy with the POPS, the CPC TSI 3007 concentration enables to measure the aerosol concentration in the 10-150 nm size range,

which is indicative of grown nucleated particles, and fine marine primary aerosols (size range 50 – 100 nm) that dominate the primary marine aerosol size distribution (Schwier et al., 2017).

2.2. Ground-based instruments

2.2.1. AERONET stations

The AERONET collaboration provides globally distributed observations of spectral AOD , inversion products, and precipitable water in diverse aerosol regimes. Aerosol optical properties are measured at multiple wavelengths ranging from the UV to shortwave infrared. AOD data (accuracy: ± 0.02) are computed for three data quality levels: Level 1.0 (un-screened), Level 1.5 (cloud-screened), and Level 2.0 (cloud screened and quality-assured) (Holben et al., 1998). For comparison with PLASMA measurements, only Level 2.0 data quality for AOD and the Angström exponent ($\alpha_{440/870}$) are used. The 2020 data from the AERONET station (St Denis) is Level 1.5. The sun-photometer we used is located on the university campus, at St Denis located in the north of the island.

2.2.2. Microwave radiometric profiler (MWRP)

The microwave profiler RPG-HATPRO G5 gives us measurements of the microwave radiation emitted by the troposphere which provides tropospheric vertical profiles (0 – 10 km) of absolute humidity and temperature, with a special focus on the MBL. It allows to monitor with a high temporal resolution (1 min) the thermodynamic state of the atmosphere and to investigate fruitfully a wide variety of weather

phenomena related to water vapour (Louf et al., 2015). A zenith-looking infrared ceilometer provides, together with the temperature profile retrieved from the MWRP, an estimate of the cloud-base height. The MWRP is also equipped with in situ sensors for ground level measurement of temperature, water vapour and pressure (Louf et al., 2015). It was on the university campus between December 12th, 2018 and March 11th, 2019.

2.3. Models and reanalyses

2.3.1. AROME

AROME-Indian Ocean (Bousquet et al., 2020) is used in this study in order to obtain the horizontal wind fields at different altitudes, at the places and dates where the flights were performed. This model is an adaptation of Météo-France's operational model AROME (Seity et al., 2011) to the Indian Ocean. AROME-IO has a horizontal resolution of 2.5 km and is initialized and coupled to the lateral limits by Integrated Forecasting System (Inness et al., 2013) operational analyzes (ECMWF, <https://www.ecmwf.int>). It is also equipped with a 1D coupling with the ocean in order to better represent the ocean-atmosphere exchanges (Bielli et al., 2021).

2.3.2. Meso-NH

Meso-NH is a non-hydrostatic mesoscale model which was developed in partnership by Centre National de Recherches Météorologiques (CNRM) and Laboratoire d'Aérodynamique (LA) and whose equations are described by Lafore et al. (1998) and Lac et al. (2018). This multidimensional model (1D, 2D or 3D) integrates a system of anelastic equations which al-

lows simulations of a wide range of meteorological phenomena from the sub-synoptic scale (a few hundred kilometers) to the microscopic scale (a few meters). In this study, the resolution used is 500 m. Meso-NH takes into account different physical aspects such as turbulence, radiation, surface processes, microphysics ... It is also coupled with gaseous, aqueous chemistry and aerosol modules which provide a privileged dynamic framework for any numerical study of atmospheric physico-chemistry.

2.3.3. FLEXPART

The FLEXPART Lagrangian Particle Dispersion Model is a comprehensive community tool for atmospheric transport modeling and analysis. It is a Lagrangian particle dispersion model that simulates the transport, diffusion, dry and wet deposition and radioactive decay of tracers released from point, line, surface or volume sources. FLEXPART can be used forward in time to simulate the dispersion of tracers from their sources, or backward in time to determine their potential source contributions (Stohl et al., 2015). In our study, FLEXPART was used to determine the back-trajectories of particles in order to know their origin. Lagrangian particle models calculate the trajectories of a large number of so-called particles (which do not necessarily represent real particles, but infinitely small patches of air) to describe the transport and diffusion of tracers in the atmosphere. FLEXPART's source code and a manual are freely available from the internet page <https://www.flexpart.eu/>. Recently, FLEXPART has been coupled to the Eulerian models AROME

248 (Verreyken et al., 2019). In this paper, we also use a ver-275 years period, the distribution and variability of marine aerosols
 249 sion of FLEXPART that has been coupled to meteorological-276 in the southern Indian Ocean {10°S - 40°S ; 50°E - 110°E},
 250 output from Meso-NH. 277 by means of satellite data (POLDER and CALIOP), CAMS

251 2.3.4. CAMS reanalyses 278

252 Copernicus Atmosphere Monitoring Service (CAMs, pre-279 sun-photometer located in St Denis (Reunion Island). They
 253 viously MACC, <https://atmosphere.copernicus.eu/>) is an at-280 found that aerosols are mainly located below 2 km a.s.l and
 254 mospheric model that simulates the mixing ratios of various 281 they estimated that SSA represents 60% to 80% of the to-
 255 aerosols, *AODs* or thermodynamic parameters (for example 282 tal *AOD*, while sulphate and Organic Matter (OM) aerosols
 256 humidity, wind, temperature ...) on a large scale and regional 283 have low contributions.

257 scale. The data assimilation system used for CAMS is based 284 For example, Figure 1 shows the CAMS mixing ratios
 258 on the ECMWF' Integrated Forecast System (IFS). Satellite 285 for March 22th, 2019 at 850 hPa ($z \approx 1.5$ km a.s.l). We ob-
 259 observations are implemented in this model and allow the 286 serve, in agreement with Mallet et al. (2018), that SSA domi-
 260 study of the atmospheric composition (chemically reactive 287 nate the aerosol loading in the southwestern Indian Ocean re-
 261 gases, aerosols, greenhouse gases) at global scale (Morcrette 288 gion, while sulfates and OM (hydrophilic) appear in smaller
 262 et al., 2009). CAMS allows in particular to differentiate vari- 289 amounts, and dust aerosols are negligible. The large-scale
 263 ous types of aerosols such as: (i) Sea Salt Aerosols (0.03-0.5 290 situation for this date is representative of the different days
 264 μm ; 0.5–5 μm and 5–20 μm) and Dust aerosols (0.03–0.55 291 of the AEROMARINE field campaign.

265 μm ; 0.55 – 5 μm and 5 – 20 μm) divided into three size 292 Figure 2 shows the CAMS mixing ratios η_{SSA} (for three
 266 ranges, (ii) Black Carbon and Organic Matter divided into 293 ranges of different SSA sizes $R_{SSA} = 0.03, 0.5, 5, \text{ and } 50 \mu\text{m}$)
 267 two modes (hydrophobic and hydrophilic) and (iii) Sulfate. 294 corresponding to the days and location of (or around) the
 268 In our study, we use the mixing ratios of these different 295 flights of the AEROMARINE field campaign. These mix-
 269 species (Mallet et al., 2018) as well as the *AOD*. Mixing ra- 296 ing ratios have been converted from kg/kg into a SSA num-
 270 tios and aerosol concentrations are directly related, allowing 297 ber concentration $\#/ \text{cm}^3$ (Table 1) in order to better compare
 271 comparison between *in-situ* measurements and CAMS data. 298 with further *in situ* (POPS, MAGIC and TSI) measurements.

272 3. Results 299

273 3.1. From global to local scale 300

274 Mallet et al. (2018) investigated statistically, over a 8- 301 sion is as follows. We first calculated the mass of SSA (in kg)
 302 where $\rho_{SSA} \approx 1183 \text{ g/cm}^3$ is a typical mass density of SSA
 303 (Bozzo et al., 2020) and N_{SSA} is the number of SSA par-

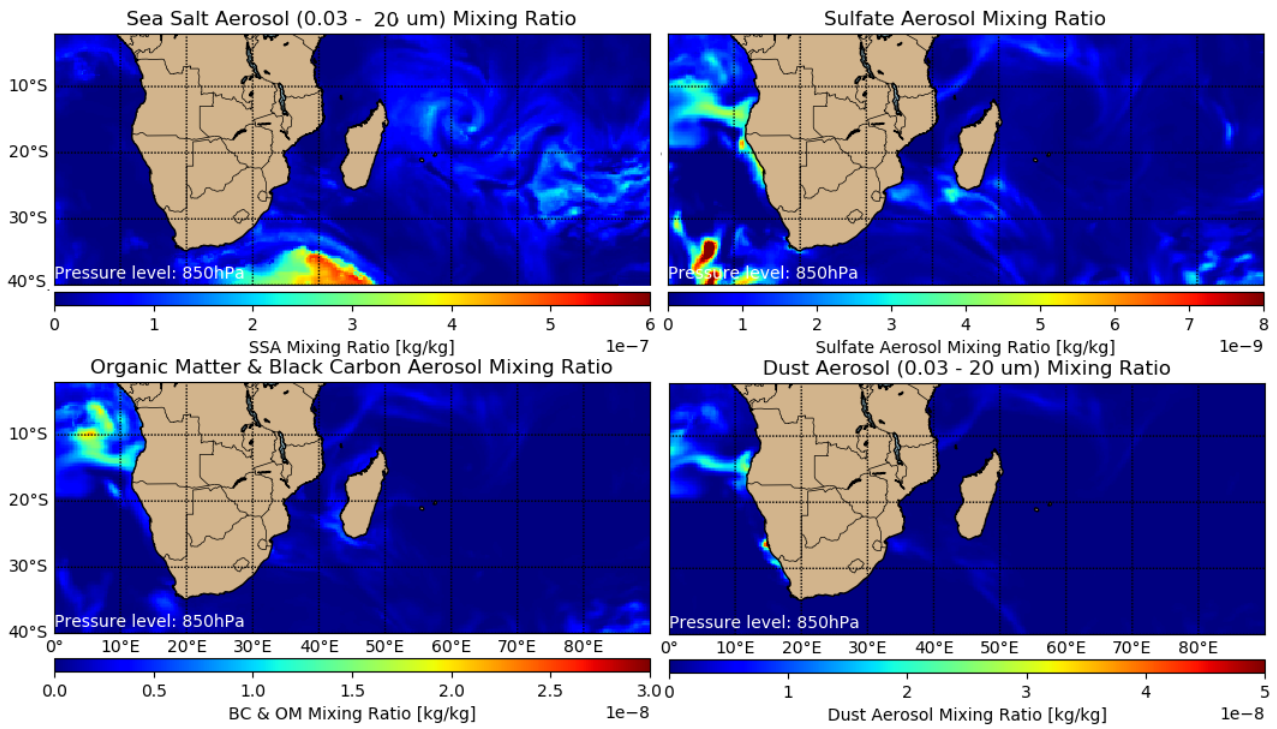


Figure 1: CAMS reanalysis (0.25°/0.25°): mixing ratio of SSA 0.03-20 μm (top left), sulfate (top right), Organic Matter and Black Carbon (bottom left) and Dust Aerosols 0.03-20 μm (bottom right) at 850hPa. Date: 03/22/2019 at 06:00:00 UTC.

304 ticles. Then, the ideal gas law gave us the volume occu-319
 305 pied by 1 kg of dry air at standard temperature T and pres-320
 306 sure p , i.e. $V = m_{air}RT/(pM)$, where $M \approx 29 \text{ g mol}^{-1}$ 321
 307 $R \approx 8.314 \text{ J K}^{-1} \text{ mol}^{-1}$. Since $\eta = m_{SSA}/m_{air}$, it ensues322
 308 directly $N_{SSA}/V = 3pM \eta_{SSA}/(4\pi R_{SSA}^3 RT \rho_{SSA})$. 323

309 The results of this conversion are summarized in Table
 310 1. These orders of magnitude are realistic values. Another
 311 precise approach would be to consider a size distribution if 325
 312 it were fully available. The POPS, TSI and MAGIC size 326
 313 ranges of measurements (respectively 132 nm–3 μm , < 10 nm 327
 314 and < 2 nm) correspond to the two smallest size ranges of the 328
 315 CAMS reanalyses (SSA between 0.03 μm and 5 μm). The 329
 316 CAMS concentrations retrieved (SSA_{0.03–0.5 μm} and SSA_{0.5–5 μm}) 330
 317 are of the same order of magnitude as the concentrations 331
 318 measured by POPS, TSI and MAGIC (see Tab.1). The largest 332

SSA concentrations (SSA_{5–20 μm}) are negligible compared to
 the other two CAMS size ranges.

We note for these flights that the SSA are not located on
 the same side of Reunion Island depending on the day. We
 will see later that this is explained by the wind regimes.

3.2. Thermodynamic parameters

Figure 3 present the averaged profiles (for March 2019)
 of the relative humidity and the temperature resulting from
 the measurements made by the MWRP and by the CAMS
 reanalyses.

The radiometer and CAMS reanalysis are in agreement
 on the relative humidity values between 0 and 1 km a.s.l.,
 with a surface value of 70% and a maximum of 80% around

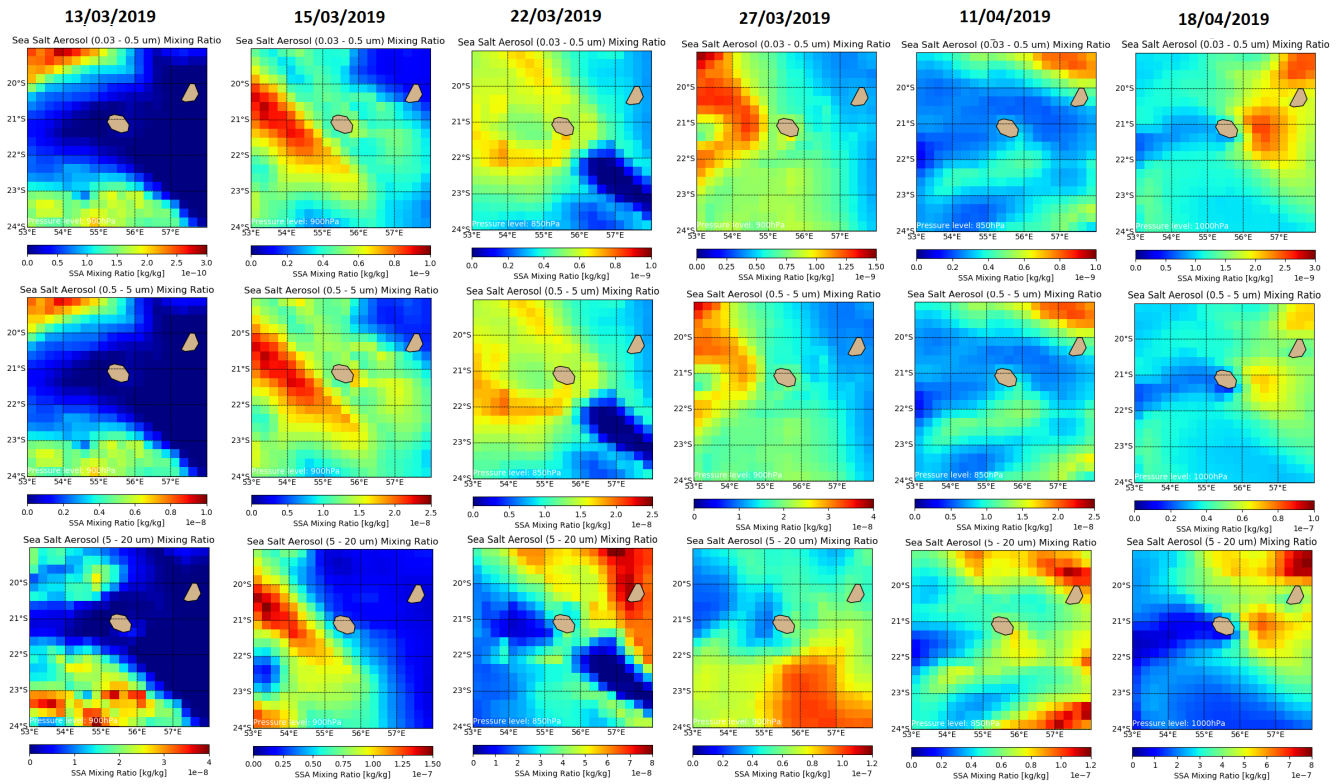


Figure 2: CAMS reanalysis ($0.25^\circ/0.25^\circ$): mixing ratio of SSA 0.03-0.5 μm , SSA 0.5-5 μm , and SSA 5-20 μm (from top to bottom) on 03/13/2019, 03/15/2019 (at 900 hPa), 03/22/2019 (at 850 hPa), 03/27/2019 (at 900 hPa), 04/11/2019 (at 850 hPa) and 04/18/2019 (at 1000 hPa) from left to right.

Table 1

Range of concentrations measured by POPS, TSI and MAGIC and range of SSA concentrations (size ranges: 0.03-0.5 μm ; 0.5 – 5 μm and 5 – 20 μm) from CAMS reanalyses in the pixel where the flight took place, for the six flight dates.

| Date | MAGIC ($\#/cm^3$) | TSI ($\#/cm^3$) | POPS ($\#/cm^3$) | SSA _{0.03-0.5μm} ($\#/cm^3$) | SSA _{0.5-5μm} ($\#/cm^3$) | SSA _{5-20μm} ($\#/cm^3$) |
|-------|---------------------|-------------------|--------------------|---|--|---|
| 03/13 | 200 to 2.10^3 | 100 to 10^3 | 5 to 100 | 0.3 to $1.4.10^3$ | $1.2.10^{-3}$ to 0.1 | $4.6.10^{-4}$ to 0.03 |
| 03/15 | 200 to 300 | 100 to 200 | 50 to 100 | 2.3 to $1.0.10^4$ | 0.06 to 60 | $3.7.10^{-3}$ to 0.2 |
| 03/22 | - | 10 to 300 | 32 to 100 | 3 to $1.3.10^4$ | 0.08 to 76.3 | $2.8.10^{-3}$ to 0.2 |
| 03/27 | 500 to 2.10^3 | 200 to 10^3 | 30 to 130 | 4.1 to $1.9.10^4$ | 0.01 to 12.1 | $1.8.10^{-3}$ to 0.1 |
| 04/11 | 800 to 8.10^3 | - | 74 to 130 | 2.4 to $1.1.10^6$ | 0.06 to 58.7 | $5.5.10^{-3}$ to 0.4 |
| 04/18 | 200 to 2.10^4 | - | 7 to 132 | 6.0 to $2.7.10^4$ | 0.2 to 180 | 0.02 to 1.2 |

333 0.5 to 1 km in altitude. However, above 1 km a.s.l, CAMS³³⁶ reanalyses and radiometer measurements are very close to
 334 reanalyses underestimate the relative humidity from 5% at³³⁷ each other.
 335 2 km to 20% at 5 km altitude. For the temperature, CAMS³³⁸ From the radiometer measurements, we observe that rel-

Table 2

Availability of instruments during flights (F1 to 6).

| AVAILABLE INSTRUMENTS | | | | |
|-----------------------|--------|-------|------|-----|
| Flight | PLASMA | MAGIC | POPS | TSI |
| F1 | ✓ | ✓ | ✓ | ✓ |
| F2 | ✓ | ✓ | ✓ | ✓ |
| F3 | ✓ | ✓ | ✓ | ✓ |
| F4 | ✓ | ✓ | ✓ | ✗ |
| F5 | ✓ | ✓ | ✓ | ✗ |
| F6 | ✓ | ✓ | ✓ | ✓ |

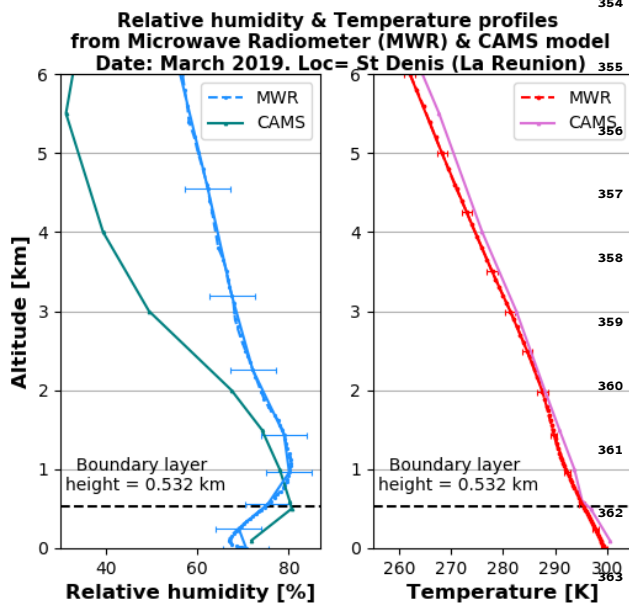


Figure 3: Average profiles of temperature and relative humidity from microwave radiometer and from CAMS reanalysis (20.8°S; 55.2°E) for March 2019.

tion under marine conditions.

3.3. The AEROMARINE field campaign

The AEROMARINE field campaign allowed to better understand the 3D distribution of marine aerosols around Reunion Island and how it is influenced by the dynamics of the MBL thanks to an instrumental synergy: PLASMA, POPS, Tandem CPC TSI3007 and MAGIC200 (Table 2). Six flights, of a duration of about ninety minutes, allowed to sample the aerosols from an altitude of 100 m up to 4 km and up to about 2 km off the west coast. The flight paths are shown on Fig. 4. They were designed to have most of the time a vertical profile above the ocean, and to measure air masses above the Maïdo mountain on the way back to the airport. Since focus is put on marine aerosols, we are going to divide these flights into two groups: (I) when only the ascending part is over the ocean (F1, F2, F3) and (II) when the whole flight is over the ocean (F4, F5). Finally, flight F6 is treated separately since the plane flew over the city of St Denis (red box on Fig 4). We will see that this flight is interesting to segregate data between land/ocean conditions.

3.3.1. Optical properties from PLASMA measurements

Figure 5 displays the *AOD* and α vertical profiles measured by PLASMA during each flight. For group II, we have separated the ascending phase from the descending phase. For each flight and for each wavelength, the *AOD* is lower than 0.1 during the ascending phase, with values below 0.05 between 500 m and 1 km, and up to 1.5 km for flight F5.

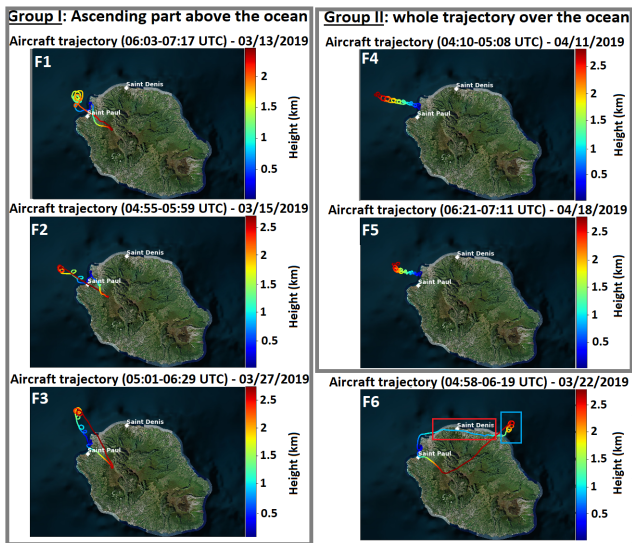


Figure 4: Flight trajectories and altitudes on 03/13/2019, 03/15/2019, 03/27/2019 (Group I) and 04/11/2019, 04/18/2019 (Group II). The sixth flight is a particular case (see text for details).

est wavelengths (380, 440 nm) show the highest *AOD*. This suggests that the sampled atmosphere was made of particles with size of the order of, or comparable to, these wavelengths, so particles rather in the accumulation mode, with the exception just mentioned which could indicate the presence of larger particles.

α (Angström exponent) is a good qualitative indicator of the mean size of the sampled aerosols. The PLASMA measurements reveal that α is lower than 1.2, independently of the altitude. This clearly suggests the presence of marine aerosols like sea salt (Schuster et al., 2006), since the CAMS retrievals (Fig. 1) indicate that the contribution of dust aerosols were negligible. For group I, α presents in general a maximum around 1.0 within the 0.5–1.5 km a.s.l layer. Regardless of local maxima in α that corresponds to sudden and localized changes in the corresponding *AOD*, the overall behaviour of α with altitude suggests that the larger particles are situated between 0.5 – 1.5 km. For flight F1, α reaches a maximum of 1.5 at about 800 m in altitude, in agreement with the peak in *AOD* at 440 nm and the almost null value of *AOD* at 1020 nm, indicating the presence of smaller particles at this altitude.

For group II, the ascent profiles share similar characteristic to those from group I with an increase of α with the altitude up to 1.5 km and a slight decrease above. The values of α vary between 0.6 and 1.2. However, larger particles seems to occupy the altitudes above 1.5 km compared to group I. Below 1.5 km, a decrease of 0.5 can be found in α values between the descent (< 0.5) and ascent phases, which could

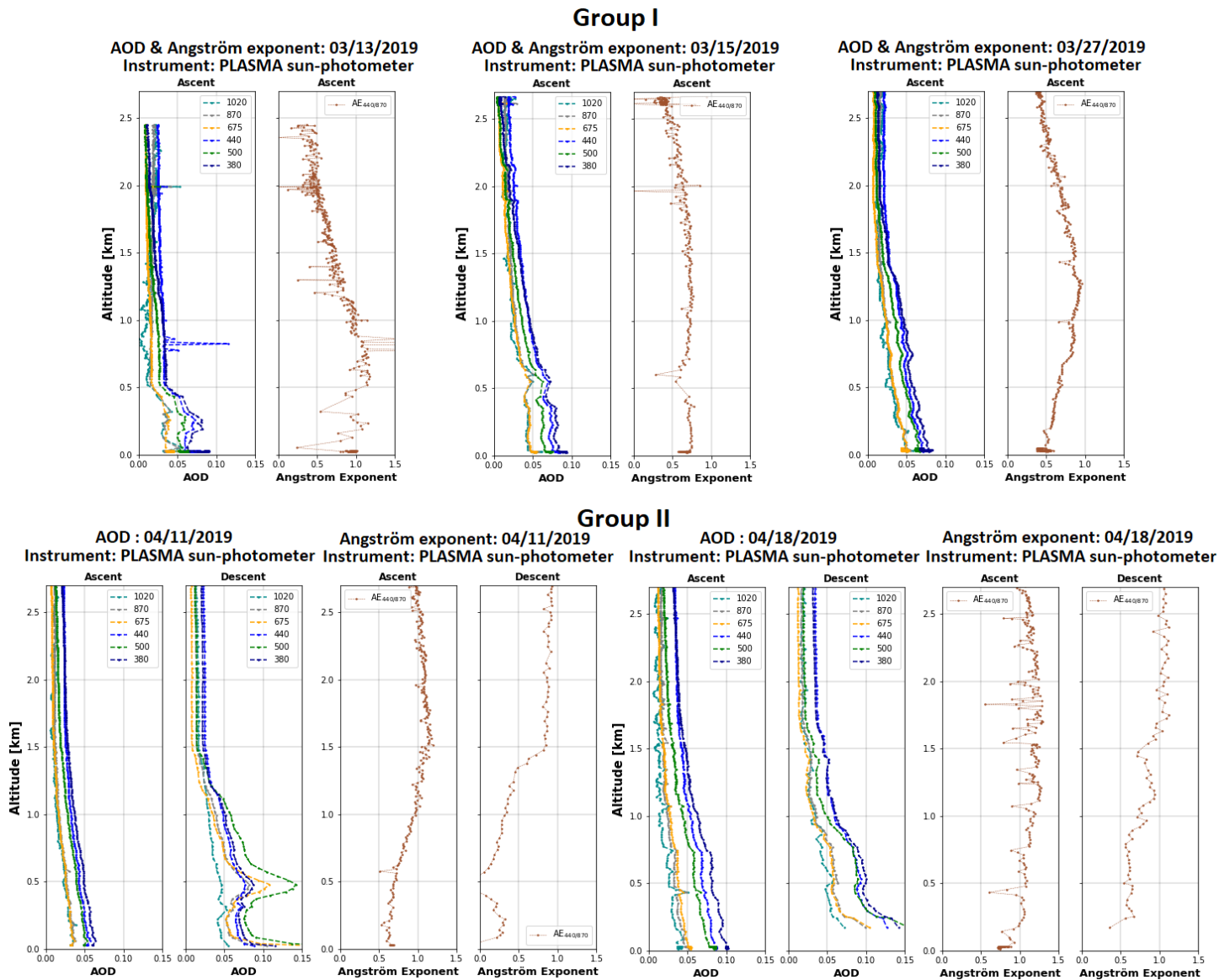


Figure 5: AOD and Angström exponent (α) vertical profiles (PLASMA measurements) for flights F1, F2, F3 (Group I) and flights F4, F5 (Group II).

417 indicate a depletion of small particles in favor to larger ones 424 number concentrations of around 10^2 cm^{-3} between 0.5 and

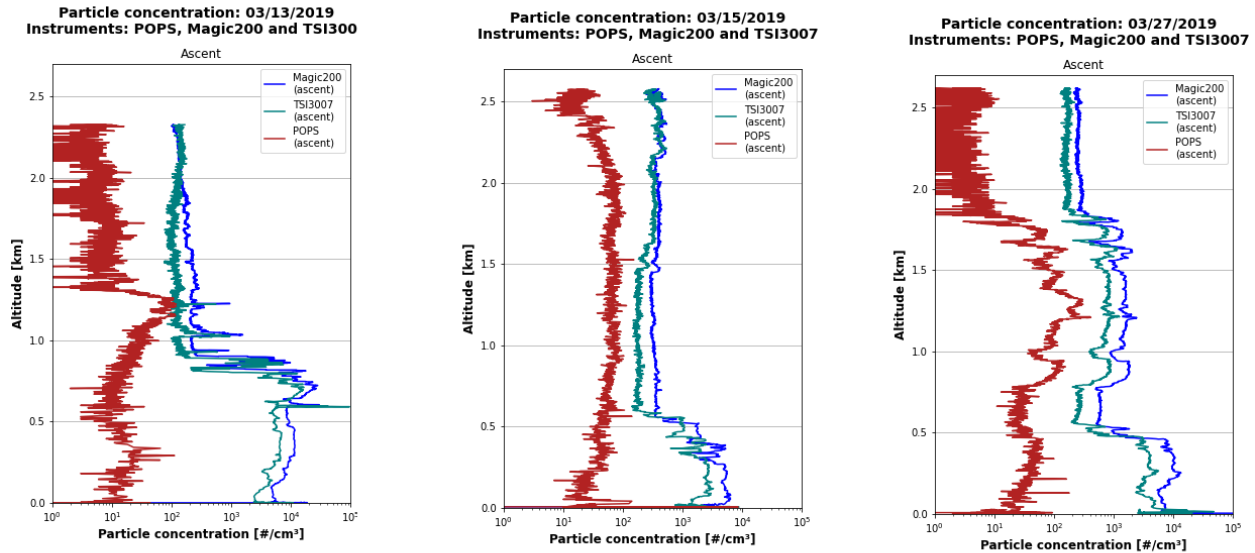
418 **3.3.2. Aerosol concentration measurements**

419 Figure 6 presents the aerosol concentration measurements
 420 by MAGIC (particle size larger than 2.5 nm), TSI (particle
 421 size larger than 10 nm) and POPS (particle size larger than
 422 132 nm). POPS concentration profiles show that the sampled
 423 particles (accumulation and coarse modes) have a maximum

425 1.5 km, and around 10 to $3 \times 10^2 \text{ cm}^{-3}$ above. It confirms
 426 that larger particles are found between 0.5 and 1.5 km in al-
 427 titude, in agreement with the conclusions deduced from the
 428 optical measurements. Below 0.5 km a.s.l, the POPS con-
 429 centrations increase with altitude during the ascent phase.

430 The shape of the measured concentration profile can show
 431 a maximum (group I) or a minimum (group II) in the layer

Group I



Group II

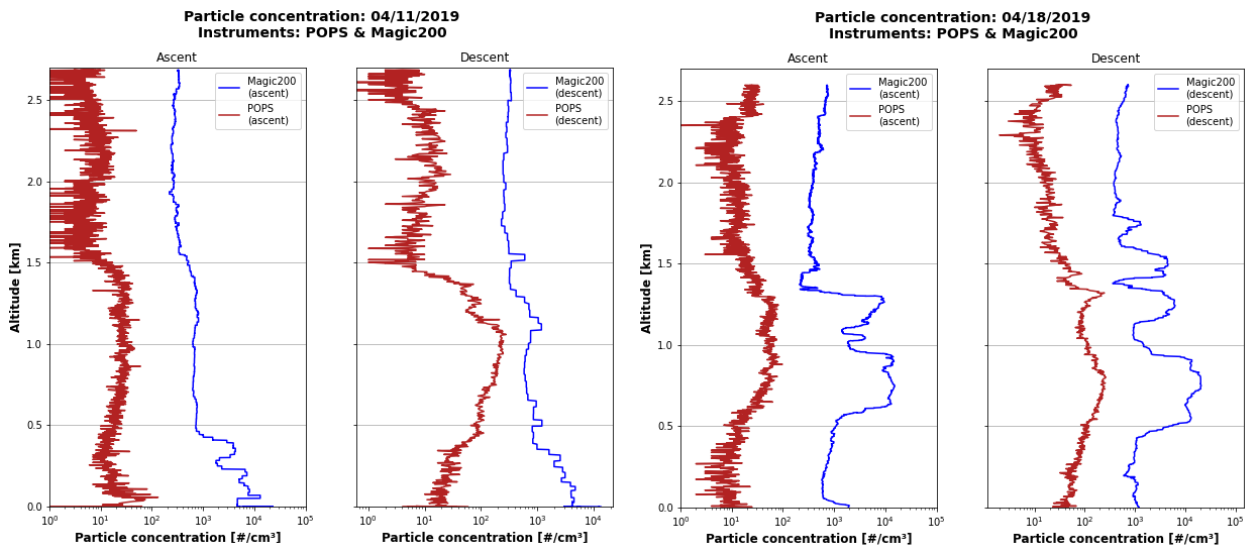


Figure 6: Particle concentration profiles (from POPS, TSI3007 and MAGIC200 instruments) during F1, F2, F3 (Group I) and F4, F5 (Group II).

432 below 0.5 km. During the descent (group II), the POPS con-438
 433 centrations decrease with altitude between the surface and 439
 434 0.5 km. Furthermore, the aerosols concentrations are higher 440
 435 between 1 and 1.5 km a.s.l compared to the ascent phase, up 441
 436 to a factor of 10 for flight F4 at 1 km a.s.l. Above 1.5 km a.s.l. 442
 437 the POPS profiles during the ascent and descent phases are 443

in agreement, with similar shapes and concentrations. POPS counts more particles during the descending phase of the flight. This is tempting to explain this increase by physico-chemical processes that would modify the aerosol number or the aerosol size so that small particles became large enough to be counted by POPS. However, we have to keep in mind

444 that the trajectory of the plane during the descent is the same 473 time to develop a bit more.

445 as the ascending trajectory, so we cannot exclude an influ- 474 For flight F1, the MAGIC and TSI concentration profiles
446 ence of the plane in the aerosol content when coming back 475 are rather constant at $2 \cdot 10^2 \text{ cm}^{-3}$ above 1 km. For flight F2,
447 Also, we cannot totally exclude that the air mass has changed 476 the concentrations are constant above 1.5 km at $4 \cdot 10^2 \text{ cm}^{-3}$.
448 by advection between the ascent and the descent of the plane 477 For flight F3, a value of $4 \cdot 10^2 \text{ cm}^{-3}$ is found above 2 km,
449 Comparing the aerosol concentrations measured by POPS 478 and a value of 10^3 cm^{-3} is found in the layer between 0.8
450 to the measurements from MAGIC and TSI will help fur- 479 and 1.6 km.

451 ther evaluate the vertical distribution of aerosols according 480 For group II, only MAGIC was available. Similar fea-
452 to their size. Differences in TSI and MAGIC concentra- 481 tures can be found in the profiles of flights F4 and F5 com-
453 tions are minimum above 1.5 km a.s.l. In particular, their 482 pared to group I. Furthermore, contrary to the aerosol con-
454 values are almost identical above 1.5 km a.s.l for flight F2, 483 centration measured by POPS, the aerosol concentrations are
455 and above 2. km a.s.l for flight F1. Below those altitudes, 484 rather similar between the ascent and descent phases.

456 the MAGIC concentrations are around twice those of TSI 485 Other important information are obtained when compar-
457 This means that small particles (nucleation mode) are twice 486 ing the POPS and MAGIC profiles. Indeed, the concen-
458 (in concentration) than larger particles (Aitken mode) below 487 tration profile differences “MAGIC - POPS” (not shown)
459 1.5 km while above, there is no small particles (MAGIC-TSI 488 present relatively smaller values above 0.5 km. More sig-
460 ratio close to one). Such values of number concentration in 489 nificant differences are obtained below this altitude. An ex-
461 the nucleation mode, between 10^3 and 10^4 cm^{-3} , have been 490 ception occurs for flight F1 since the critical altitude is 1 km
462 measured also in the Mediterranean (Eleftheriadis et al., 2006). 491 because of a more developed boundary layer, as already sug-
463 For the flights in group I, the concentration vertical pro- 492 gested above. Another exception is for flight F5 where sig-
464 files obtained from MAGIC and TSI present similar shapes 493 nificant differences are between 0.5 and 1.5 km and small
465 On average, MAGIC concentrations are 2 to 3 times higher 494 differences elsewhere. For group II, no significant differ-
466 than TSI concentrations. The highest concentrations are found 495 ences are noted between the ascent and the descent *i.e.* same
467 in the marine boundary layer below 0.7 km a.s.l for flight 496 shape and order of magnitudes in the concentration profile
468 F1, and below 0.5 km a.s.l for flight F2 and F3, with val- 497 differences.

469 ues ranging from 2000 to 10000 cm^{-3} . This difference of 498 In summary, the measurements indicate that the bound-
470 200 m in the marine boundary layer may be due to the fact 499 ary layer below 0.5 km – 0.7 km is much richer in aerosols
471 that flight F1 occurred one hour later in the morning com- 500 in the nucleation or Aitken modes (size lower than 132 nm).
472 pared to flights F2 and F3, so the boundary layer may hav- 501 Above the boundary layer, and up to 1.5 km to 2 km depend-

ing on the flight, these modes have a lower concentration and larger particles (size greater than 132 nm - accumulation mode) are dominant. The exception in the marine boundary layer for flight F5, *i.e.* below 0.5 km, means that this layer is poorer in terms of small aerosols.

3.3.3. Origin of the air masses

To further evaluate the origin of the air masses identified in the previous section, we used FLEXPART mesoscale backtrajectories to distinguish air masses influenced by local terrestrial emissions from those with marine origin or representative of the regional background. Here, we have chosen a backtime of 12 h because it corresponds to the domain of AROME.

The tables A1 and A2 in the appendix presents statistical products from the FLEXPART output.

The scientific meaning of the FLEXPART outputs needs to be briefly reminded in order to avoid misunderstandings about the result presented in those tables. When we release an air mass at a given altitude z_r , FLEXPART is able to trace back its probable trajectories, over a geographical grid, during an user-decided time interval. From that, it is then possible to identify (and reckon) the oceanic pixels, *viz.* the trajectory grid-points located over the ocean, and similarly for the island pixels which are trajectory grid-points located over Reunion Island. In other words, we can quantify how much could the ocean contribute to, or impact, the aerosol content of the considered air mass.

Beside the geographic origin, it is possible to determine

the tropospheric layer from where an air mass originates. The results from the previous sections helped us identify three layers: (L1) below 0.5 km, (L2) between 0.5 and 1.5 km, and (L3) above 1.5 km. For instance, in Table A1, the results after 12 h of backward simulations for an altitude release at 200m for flight F1 show that 88% (first row, last column) of the air mass originated from grid cells over the ocean, and 12% from grid cells over Reunion island. In addition, the origin of the air mass can be analysed in terms of geographic location and height. Hence, 43% of the air mass originated from 0-500m in altitude (layer L1), 38% from 500 to 1500m in altitude (layer L2), and 7% above 1500m (layer L3) and above the ocean. Therefore, the origin of this air mass is mainly oceanic.

We have thus used FLEXPART to calculate the origin of air masses from different altitudes. For group I, we can see that the origin of the air masses is mainly oceanic since more than 73% of the backtrajectories originate from grid cells above the ocean.

In contrast, 28% of the air mass was located above Reunion island, and within the layer L2 and L3. For group II, the results are different since the air masses present a significant origin above Reunion island. In particular, the air masses released at the 200 m and 1 km altitudes for flight F4 have a dominant origin above Reunion island.

Comparing the altitude where the backtrajectories are released, and the distribution in the vertical of the backtrajectories give additional information on the vertical transport between layers. Let us first look at oceanic pixels for group

I. First, we note that the air masses with a dominant marine origin stayed, for a large part, within the same layer they originated from. For example, for a release at 200 m, 43% of the air mass with marine origin were in the layer L1. Excepted for some rare exceptions (underlined in tables), the layer that presents the highest percentages (in bold fonts in tables) includes the altitude of release. However, exchanges of air masses (in italic fonts in tables) between layers are not negligible, even if they are not dominant. For instance (flight F1), for a release at 1 km, 29% of the air mass with marine origin come from the layer L1. This means that the aerosol content in the lower troposphere is also impacted by the mixing between contiguous layers. This result holds for the air masses originating from Reunion island, although the terrestrial component in the lower troposphere is mostly significant in the layer L2 (percentages greater than 10%). For the group II flights, we have the same results although we recognize that the insular influence is more present, especially at low level for flight F4. This may be correlated with MAGIC and PLASMA measurements. Indeed, for flight F4 the maximum MAGIC concentrations are measured below 0.5 km a.s.l, which corresponds to a majority of island pixels in the Table A1. It is also at this altitude that PLASMA measures the most important AODs (during the descending phase).

We are summarized with typical orders of magnitude the results given in Tables A1 and A2. These conclusions are summarized on Figure 7. The vertical layering we found and in particular the predominance of the oceanic aerosols

are explained by the interaction between the wind field and Reunion island's complex terrain. The AROME model outputs (not shown) reveal a dominant south-west and south wind weather regime occurred over the sea at the time of the flights, with sometimes strong recirculation on the lee side, off the west coast of Reunion Island.

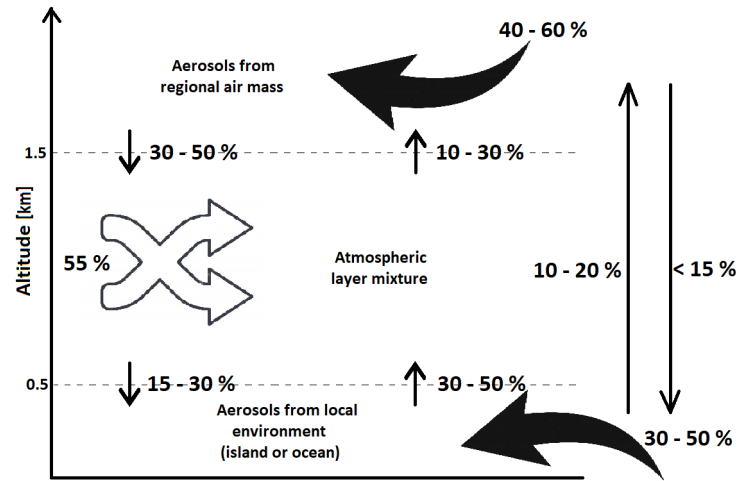


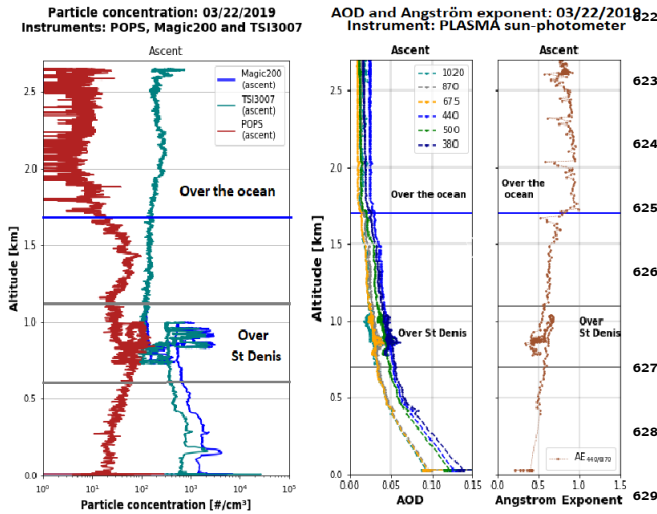
Figure 7: Descriptive diagram of aerosols inputs and the exchanges between the atmospheric layers L1 (below 0.5 km), L2 (0.5 – 1.5 km) and L3 (above 1.5 km).

3.3.4. Special case: flight of 22 March 2019 (F6)

This flight (F6) is of particular interest since the plane flew over St Denis between 05:20 and 05:30 UTC at an altitude of about 900 m (red box on Fig.4), then ascended in spirals above the ocean up to 2.5 km (blue box on Fig.4). It finally flew over St Paul before landing.

The measured AODs and α over St Denis (grey boxed area on Figure 8) have a local maximum of 0.05 and minimum of 0.5 respectively, while over the ocean (blue box in fig.8), the measured AODs are constant ($AOD < 0.05$) and α is around 0.8 – 1. This suggests that smaller particles are

605 sampled when the plane is over St Denis.



606 **Figure 8:** Particle concentration profiles from POPS, TSI3007
607 and MAGIC200 instruments (left), AOD and Angström expo-
608 nent ($\alpha_{440/870}$) profile from PLASMA sun-photometer (right)
609 during flight on 03/22/2019 (F6).
610

611 The difference in concentration between MAGIC and POPS
612 is much larger over St Denis than over the ocean. This means
613 that, as indicated by the PLASMA optical measurements,
614 small particles (size lower than 132 nm) are the dominant
615 mode over St Denis. The MAGIC - TSI differences in con-
616 centration further indicates that the smallest particles are those
617 that dominate. In contrary, the MAGIC - TSI difference
618 is close to zero and confirm that larger particles are found
619 above 1.5 km a.s.l over the ocean north east of the island.

620 The wind direction given by AROME (not shown here)
621 indicate (i) at 1 km (overflight of St Denis) a southeast wind
622 of around 10 m s^{-1} coming from the island and (ii) at 1.5 km,
623 when the plane begins these spirals above the ocean, a south-
624 east wind from the ocean with a speed of about 8 m s^{-1} .

625 The FLEXPART backtrajectory results (table A2 in the

626 appendix section) indicate that for a release at 1.5 km, the air
627 mass origin was purely marine and stayed above 500m over
628 the past 12 hours. This is due to a southeasterly wind regime,
629 according to AROME wind fields (not shown). Hence, the
630 layer at 1.5km in altitude is representative of the regional
631 background.

632 3.4. Comparisons with other databases

633 3.4.1. Comparison with AERONET measurements

634 Assuming that the AOD is mostly influenced by ma-
635 rine aerosols on the north and west shore, one can compare
636 AOD measured by the AERONET station at St Denis and
637 the AOD measured by PLASMA on the runway.

638 Table 3 brings together the mean values of the AOD
639 $_{500nm}$ on the runway (before takeoff) measured by PLASMA
640 and the AOD $_{500nm}$ measured by the AERONET sun-photometer
641 (St Denis) at the same time. Both the AOD and α from
642 AERONET and PLASMA are in agreement for flights F2,
643 F3 and F4. For the flight F1, the AERONET sun-photometer
644 measures a larger Angström exponent while for flights F5
645 and F6 it is the AODs measured on the runway by PLASMA
646 which are larger. However, these differences are consistent
647 with the accuracy of the two photometers (AERONET: ΔAOD
648 $= \pm 0.02$ and PLASMA: $\Delta AOD = \pm 0.005 - 0.01$ according
649 to λ). The exception of the flight over St Denis (flight F6)
650 where $AOD_{AERONET} > AOD_{PLASMA}$ can be explained
651 by the difference in altitude of the two measurements (0.9 km
652 for PLASMA and ground-based for AERONET).

653 So AERONET measurements are generally in agreement

Table 3

AOD at 500nm and Angström exponent (α) on the runway from the PLASMA sun-photometer and from the AERONET sun-photometer (St Denis) for each flight date

| Flight | PLASMA | | AERONET | |
|----------------|-----------------------------|---------------|-----------------------------|---------------|
| | <i>AOD</i> _{500nm} | α (AE) | <i>AOD</i> _{500nm} | α (AE) |
| F1 | 0.06 | 1.0 | 0.06 | 1.7 |
| F2 | 0.07 | 0.6 | 0.07 | 0.7 |
| F3 | 0.07 | 0.5 | 0.06 | 0.4 |
| F4 | 0.05 | 0.6 | 0.04 | 0.7 |
| F5 | 0.09 | 0.6 | 0.06 | 0.6 |
| F6 | 0.12 | 0.4 | 0.06 | 0.4 |
| Over St D.(F6) | 0.04 | 0.5 | 0.07 | 0.2 |

marine station.

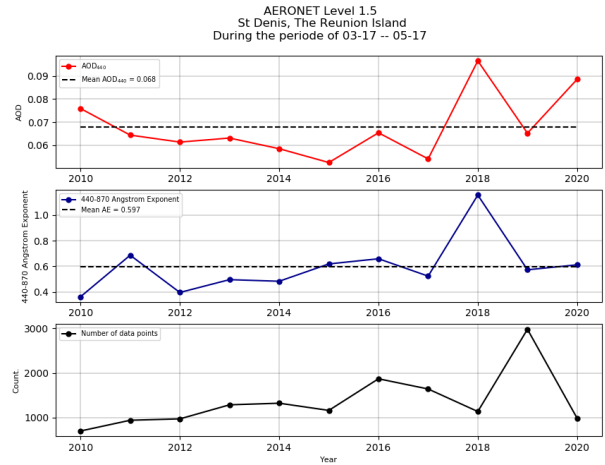


Figure 9: Mean *AOD*, mean α and number of data points from AERONET station in St Denis (Level 1.5) for the period from March 17 to May 17 (2010 - 2020).

3.4.2. Comparison with CAMS reanalyses

Figure 10 presents the daily *AOD* averages of the CAMS model (model grid point: 20.8°S; 55.2°E) and of the AERONET sun-photometer (St Denis) for March and April 2019. Over this period, CAMS overestimates the *AOD* by 0.03.

Daily differences between CAMS reanalyses and AERONET measurements are presented in Table 4 (values rounded to the hundredth). The monthly averages of the *AODs* given by the CAMS reanalyses is 0.11, for March and April 2019. The monthly averages of the *AODs* measured by the AERONET sun-photometer is 0.08 for March and April 2019. This shows an overestimate of CAMS of 0.03 for March and April 2019. In particular, the CAMS reanalyses overestimate the *AODs* from 0.03 to 0.09 for flights F1, F3, F4 and F6. The difference between CAMS and the PLASMA AERONET sun-photometer is statistically insignificant for flights F2 and F5.

These results agree with those obtained by Mallet et al.

649 with those carried out during flights. If one relies on the 667
 650 AERONET retrievals, the general agreement with the PLASMA 668
 651 retrievals suggests that PLASMA offered a representative 669
 652 sampling of the aerosol content around Reunion Island. We 670
 653 further evaluated this by comparing the *AOD* AERONET 671
 654 measurements before and during the 2020-lockdown due to 672
 655 the Covid19 pandemic, assuming that the terrestrial sources 673
 656 were similar between both periods. Reunion Island experi- 674
 657 enced a lockdown between 17 March 2020 and 17 May 2020 675
 658 and hence mobile traffic and anthropogenic activities were 676
 659 reduced. The three plots presented in Fig 9 show that no 677
 660 statistically significant change in the *AOD* or Angström ex- 678
 661 ponent can be clearly attributed to the lockdown. This tends 679
 662 to indicate that indeed the AERONET station at St Denis is 680
 663 not significantly impacted by local anthropogenic aerosols 681
 664 and confirms the results of Hamill et al. (2016) that it is a 682

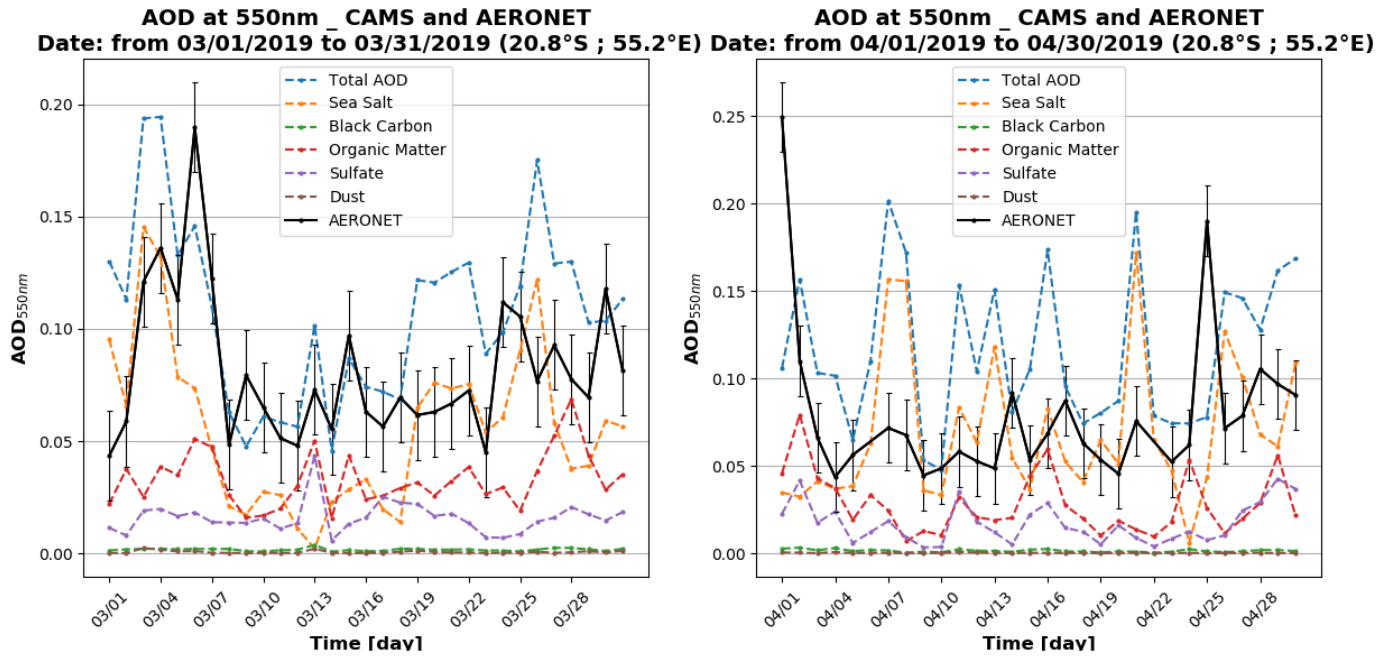


Figure 10: AOD measurements from AERONET sun-photometer (Level 1.5) and from CAMS reanalysis (20.8°S; 55.2°E) for March 2019 and April 2019.

Table 4

Differences in daily AOD averages of the CAMS model (20.8°S; 55.2°E) and of the AERONET sun-photometer (St Denis) for each flight

| Flight | $AOD_{CAMS} - AOD_{AERONET}$ |
|--------|------------------------------|
| F1 | + 0.03 |
| F2 | - 0.01 |
| F3 | + 0.04 |
| F4 | + 0.09 |
| F5 | + 0.01 |
| F6 | + 0.06 |

3.4.3. Comparison with Maïdo measurements

The *in situ* measurements on board the light plane in the free troposphere are further compared to the measurements from the high altitude Maïdo Observatory (21.08° S, 55.38° E; 2.2 km a.s.l). We use the measurements made by a Scantron particle counter described in Foucart et al. (2018) (concerning aerosols of size 10–600 nm) and a CPC TSI (aerosols greater than 10 nm) from the Maïdo Observatory for comparison with the in-flight data (POPS, TSI and MAGIC). Due to a complex interplay between land-sea breeze, catabatic wind and complex terrain, only the in-situ measurements Maïdo taken between 21:00 and 03:00 UTC can be considered as free tropospheric (Verreyken et al., 2021).

Figure 11 display the mensual averages for March and April 2018 for the Scantron and the TSI located at Maïdo. The time series (POPS, TSI and MAGIC measurements) dur-

(2018) who determined that the AODs given by CAMS over-estimate by about 0.05 the local AERONET measurements.

Table 5

Comparison of average nighttime concentrations (Maïdo Observatory) and concentrations in the free troposphere during flights.

| Date | Mean nighttime concentration at Maïdo D-1 (21:00-03:00 UTC) | | Concentrations during flights (in free troposphere) | | | Mean nighttime concentration at Maïdo D+1 (21:00-03:00 UTC) | |
|-------|--|-----------------------------|--|-----------------------------|-------------------------------|--|-----------------------------|
| | Scanotron (#/cm ³) | TSI (#/cm ³) | POPS (#/cm ³) | TSI (#/cm ³) | MAGIC (#/cm ³) | Scanotron (#/cm ³) | TSI (#/cm ³) |
| 03/13 | 129.7 | X | 0 - 21 | 102 - 180 | 101 - 146 | X | X |
| 03/15 | 189.7 | X | 3 - 97 | 226 - 542 | 244 - 542 | 210.8 | 247.0 |
| 03/22 | 321.4 | X | 0 - 29 | 147 - 746 | X | 143.2 | X |
| 03/27 | 268.0 | X | 0 - 12 | 126 - 221 | 213 - 302 | 190.6 | X |
| 04/11 | 129.1 | 376.4 | 0 - 50 | X | 236 - 347 | 109.7 | 346.8 |
| 04/18 | X | 548.6 | 1 - 54 | X | 379 - 771 | X | 671.0 |

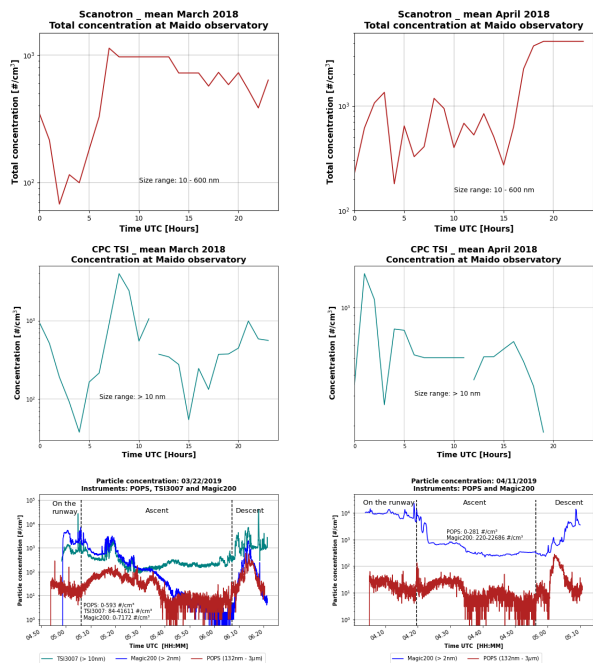


Figure 11: March and April 2018 averages of measurements at the Maïdo Observatory by the Scanotron and the CPC TSI and time series of concentrations measured during the flights of 03/22/2019 (F6) and 04/11/2019 (F4).

703
704 For March, the average TSI measurements at Maïdo and
705 during the flight have the same order of magnitude (between
706 40 and $4 \cdot 10^3 \text{ #.cm}^{-3}$). However, the POPS measurements
707 during the flight (March and April) are much lower than
708 those of the Scanotron at 2.2 km a.s.l. The Scanotron (10 –
709 600 nm) measures aerosols smaller than the POPS (132 nm
710 - $3 \mu\text{m}$). This would mean that the majority of the aerosols
711 measured above 2.2 km a.s.l are less than 132 nm (in agree-
712 ment with CAMS section 3.1).

Table 5 presents the measurements made during flights in the free troposphere (measurements for an altitude higher than 2 km) and the average concentrations measured at the Maïdo Observatory (2.2 km a.s.l) during the nights before and after the flights, when the observatory is in the free troposphere.

Overall, the MAGIC and TSI measurements made dur-

ing flight in the free troposphere are of the same order of magnitude as the Scanotron night measurements made at the Maïdo Observatory, in the free troposphere (between 1×10^2 and $7 \times 10^2 \text{ cm}^{-3}$). The two TSI CPCs (at the Maïdo Observatory and on the plane) also measure identical concentrations above 2 km (around 10^2 cm^{-3}).

We can conclude that the nighttime measurements at the Maïdo Observatory (at 2.2 km a.s.l) are representative of the daytime measurements (during flights) in the free troposphere and allow sampling of purely marine aerosols.

4. Conclusion

In this paper, we have presented the AEROMARINE field campaign which took place between February and April 2019 off the coast of Reunion Island (southwestern Indian Ocean). This area, identified as a pristine region, is of major interest for the study of marine aerosols, their vertical distribution and their optical properties.

During this campaign, a MWRP was deployed in St Denis (93 m in the north of the Island) between mid-December 2018 and mid-March 2019. This made it possible to determine that, during the austral summer in this region, the thermodynamic situation (humidity, temperature, and height of the boundary layer) is relatively stable.

In addition, six instrumented flights allowed the aerosols to be sampled from an altitude of 100 m up to 4 km by spiraling above the ocean thanks to an instrumental synergy.

The optical properties of the aerosols were measured by the PLASMA photometer and three particle counters (POPS

TSI and MAGIC) measured the aerosol concentrations for different size ranges (accumulation, coarse and Aitken modes). POPS analysis indicates that almost all of the particles are in the accumulation mode, centered around a particle size of 132 nm.

The results obtained show *AODs* less than 0.1 (with some exceptions), which is representative of a pristine region. The various measurements (*AOD*, Angström exponents, and concentrations) also indicate that the aerosols are in the accumulation and coarse modes, and mainly below 2 km of altitude.

The FLEXPART simulations enabled to determine the most probable origin of the aerosols measured during the flights. As a result, the aerosols follow the following vertical distribution:

- Above an altitude of 1.5 km, the sampled aerosols are not substantially impacted by the surface (layer L1 has a relatively little contribution). This is interesting since it allows to quantify the background aerosol concentration. For all the flights, we have estimated that the number concentrations (in cm^{-3}) are 300 (MAGIC), 230 (TSI) and 15 (POPS). Also, the assessed AOD_{550nm} and α are respectively 0.01 and 0.75.
- Below 0.5 km (in the MBL), aerosols come essentially from the surface. The origin can be oceanic (33%) or insular (8%). Insular influence are nonetheless due to special events depending on the wind regime (*e.g.* , the Cap La Houssaye may bring sometimes dust aerosols).
- The intermediate layer, *i.e.* between 1.5 and 0.5 km

776 a.s.l, is a layer of mixture: aerosols are mixed with 805 words, measurements are not impacted by local anthropogenic
 777 those coming from the lower or upper atmospheric 806 activities and the station can be considered as representa-
 778 layers. 807 tive of marine conditions. The AEROMARINE campaign

779 These results meet the initial objectives of the AERO- 808 occurred around Reunion Island. A field campaign, Mar-
 780 MARINE campaign: (i) to characterize marine aerosol op- 809 ion Dufresne Atmospheric Program - Indian Ocean (MAP-
 781 tical properties and their vertical distribution and (ii) to ex- 810 IO), aboard the Marion Dufresne around the Terres Aus-
 782 amine the transport pathways of marine aerosols from the 811 traies Françaises (TAF) was planned for January 2021. Among
 783 MBL to the free troposphere. It is worth mentioning that 812 the objectives, one of them is to better document the ex-
 784 the flights were carried out between 04:00 and 07:00 UTC, 813 changes between the pristine Southern Indian Ocean and the
 785 viz. during the transient convection regime between noctur- 814 atmosphere. For our topic, this campaign will allow the re-
 786 nal and diurnal conditions. Further observational studies and 815 sults presented in this paper to be deepened, since it will pro-
 787 field campaign may be necessary to examine aerosol distri- 816 vide data about marine aerosol emissions and of aerosol and
 788 butions during purely diurnal and nocturnal regimes, *i.e.* for 817 humidity exchanges between the pristine ocean and the MBL
 789 well established regimes. The AEROMARINE campaign 818 far from any land. All of these data (from AEROMARINE
 790 presented here is interesting in the sense that it documents a 819 and then MAP-IO) will be helpful to feed models of water
 791 transient regime, namely a more complex regime in terms of 820 vapour-aerosols-clouds interactions. Such features will be
 792 thermodynamics compared to established ones. 821 the topic of future research.

793 The measurements taken during the flights were com-
 794 pared with the CAMS reanalyses. They showed that, like in-
 795 flight measurements, *SSAs* are predominant around Reunion
 796 Island and that aerosols are mainly located below 2 km. It
 797 was also shown that CAMS overestimates the *AODs* (from
 798 0.01 to 0.09) in this region in agreement with results from
 799 Mallet et al. (2018). In addition, a comparison between PLASMA
 800 measurements (on the runway) and the AERONET sun-photometer
 801 (located in St Denis) as well as a study on the impact of 2020-
 802 lockdown due to the Covid-19 pandemic on AERONET mea-
 803 surements were carried out. The results strongly suggested
 804 that the AERONET station is a marine station. In other 831

822 Acknowledgements

This work was supported by the French national pro-
 gramme LEFE/INSU. We are grateful to the Labex CAPPA
 (ANR-11-LABX-0005-01) which has funded this work in
 the context of the Cloud-aerosol interactions work package.

We acknowledge the ECMWF for providing freely reanaly-
 sis.

829 Acronyms

AERONET AErosol RObotic NETWORK.

AODs Aerosol Optical Depths.

- 832 **CAMS** Copernicus Atmosphere Monitoring Service. 845 .
- 833 **CPC** Condensable Particle Counter.
- 834 **MAP-IO** Marion Dufresne Atmospheric Program - Indian
835 Ocean.
- 836 **MBL** Marine Boundary Layer.
- 837 **MWRP** MicroWave Radiometer Profiler.
- 838 **OM** Organic Matter.
- 839 **PLASMA** Photomètre Léger Aéroporté pour la Surveillance
840 des Masses d'Air.
- 841 **POPS** Portable Optical Particle Counter.
- 842 **SSA** Sea Salt Aerosols.
- 843 **SST** Sea Surface Temperature.
- 844 **TAF** Terres Australes Françaises.

Appendix

FLEXPART simulations. Flights: F1, F2, F3 and F4

Table A1

Origin of air masses for L1, L2 and L3 according to a 12 hours-simulation of the FLEXPART model for F1, F2, F3 and F4.

| Group I: F1 and F2 | | | | | | | | | |
|---|---------|------------|----------|-------|---|---------|------------|----------|-------|
| FLEXPART simulation. Flight: F1. 12h-simulation | | | | | FLEXPART simulation. Flight: F2. 12h-simulation | | | | |
| Altitude | 0-500 m | 500-1500 m | > 1500 m | Total | Altitude | 0-500 m | 500-1500 m | > 1500 m | Total |
| Altitude release: 200 m | | | | | Altitude release: 200 m | | | | |
| Ocean | 43% | 38% | 7% | 88% | Ocean | 25% | 44% | 24% | 93% |
| Island | 2% | 6% | 4% | 12% | Island | 3% | 3% | 0.0% | 7% |
| Altitude release: 1000 m | | | | | Altitude release: 1000 m | | | | |
| Ocean | 29% | 37% | 11% | 77% | Ocean | 14% | 51% | 33% | 98% |
| Island | 4% | 17% | 2% | 23% | Island | 0 | 0 | 0 | 0 |
| Altitude release: 1500 m | | | | | Altitude release: 1500 m | | | | |
| Ocean | 13% | 29% | 31% | 73% | Ocean | 2% | 37% | 61% | 100% |
| Island | 3% | 19% | 15% | 27% | Island | 0 | 0 | 0 | 0 |
| Group II: F4 and F5 | | | | | | | | | |
| FLEXPART simulation. Flight: F4. 12h-simulation | | | | | FLEXPART simulation. Flight: F5. 12h-simulation | | | | |
| Altitude | 0-500 m | 500-1500 m | > 1500 m | Total | Altitude | 0-500 m | 500-1500 m | > 1500 m | Total |
| Altitude release: 200 m | | | | | Altitude release: 200 m | | | | |
| Ocean | 23% | 15% | 4% | 43% | Ocean | 33% | 28% | 6% | 67% |
| Island | 28% | 21% | 8% | 57% | Island | 4% | 14% | 13% | 33% |
| Altitude release: 1000 m | | | | | Altitude release: 1000 m | | | | |
| Ocean | 7% | 21% | 11% | 39% | Ocean | 12% | 27% | 11% | 50% |
| Island | 18% | 33% | 10% | 61% | Island | 6% | 31% | 13% | 50% |
| Altitude release: 1500 m | | | | | Altitude release: 1500 m | | | | |
| Ocean | 1% | 20% | 20% | 61% | Ocean | 1% | 15% | 23% | 41% |
| Island | 0 | 22% | 17% | 39% | Island | 5% | 27% | 24% | 59% |

FLEXPART simulation. Flights: F3 and F6**Table A2**

Same as Table A1 but for F3 and F6.

| F3 (Group I) and F6 | | | | |
|--|---------|------------|----------|-------|
| FLEXPART simulation. Flight: F3 | | | | |
| Altitude | 0-500 m | 500-1500 m | > 1500 m | Total |
| Altitude release: 200 m | | | | |
| Ocean | 43% | 38% | 15% | 96% |
| Island | 2% | 1% | 1% | 4% |
| Altitude release: 1000 m | | | | |
| Ocean | 19% | 42% | 27% | 88% |
| Island | 2% | 7% | 4% | 12% |
| Altitude release: 1500 m | | | | |
| Ocean | 8% | 41% | 39% | 88% |
| Island | 2% | 8% | 3% | 13% |
| FLEXPART simulation. Flight: F6 12h-simulation | | | | |
| Altitude release: 1500 m | | | | |
| Ocean | 0.0% | 35% | 65% | 100% |
| Island | 0.0% | 0.0% | 0.0% | 0.0% |

References

Andreae, M., Rosenfeld, D., 2008. Aerosol–cloud–precipitation interactions. part 1. the nature and sources of cloud-active aerosols. *Earth-science reviews* 89, 13–41.

Angström, A., 1961. Techniques of determining the turbidity of the atmosphere. *Tellus* 13, 214–223. doi:10.3402/tellusa.v13i2.9493.

Baray, J.L., Courcoux, Y., Keckhut, P., Portafaix, T., Tulet, P., Cammas, J.P., Hauchecorne, A., Godin-Beekmann, S., De Mazière, M., Hermans, C., Desmet, F., Sellegri, K., Colomb, A., Ramonet, M., Sciare, J., Vuillemin, C., Hoareau, C., Dionisi, D., Dufлот, V., Vérémes, H., Porteneuve, J., Gabarrot, F., Gaudo, T., Metzger, J.M., Payen, G., Leclair

De Bellevue, J., Barthe, C., Posny, F., Abchiche, A., Delmas, R., Ricaud, P., 2013. Maïdo observatory: a new high-altitude station facility at Reunion Island (21° S, 55° E) for long-term atmospheric remote sensing and in situ measurements. *Atmospheric Measurement Techniques* 6, 2865–2877. doi:10.5194/amt-6-2865-2013.

Bielli, S., Barthe, C., Bousquet, O., Tulet, P., Pianezze, J., 2021. The effect of atmosphere-ocean coupling on the structure and intensity of tropical cyclone bejisa in the southwest indian ocean. *Atmosphere* 12. doi:10.3390/atmos12060688.

Bousquet, O., Barbary, D., Bielli, S., Kebir, ., Raynaud, L., Malardel, S., Faure, G., 2020. An evaluation of tropical cyclone forecast in the southwest indian ocean basin with arome-indian ocean convection-permitting numerical weather predicting system. *Atmospheric Science Letters* 21, e950. doi:10.1002/asl.1950.

Bozzo, A., Benedetti, A., Flemming, J., Kipling, Z., Rémy, S., 2020. An aerosol climatology for global models based on the tropospheric aerosol scheme in the integrated forecasting system of ecmwf. *Geoscientific Model Development* 13, 1007–1034. doi:10.5194/gmd-13-1007-2020.

Crumeyrolle, S., Manninen, H.E., Sellegri, K., Roberts, G., Gomes, L., Kulmala, M., Weigel, R., Laj, P., Schwarzenboeck, A., 2010. New particle formation events measured on board the ATR-42 aircraft during the EUCAARI campaign. *Atmospheric Chemistry and Physics* 10, 6721–6735. doi:10.5194/acp-10-6721-2010.

Dufлот, V., Tulet, P., Flores, O., Barthe, C., Colomb, A., Deguillaume, L., Vaïtilingom, M., Perring, A., Huffman, A., Hernandez, M.T., Sellegri, K., Robinson, E., O'Connor, D.J., Gomez, O.M., Burnet, F., Bourriane, T., Strasberg, D., Rocco, M., Bertram, A.K., Chazette, P., Totems, J., Fournel, J., Stamenoff, P., Metzger, J.M., Chabasset, M., Rousseau, C., Bourriane, E., Sancelme, M., Delort, A.M., Wegener, R.E., Chou, C., Elizondo, P., 2019. Preliminary results from the farce 2015 campaign: multidisciplinary study of the forest–gas–aerosol–cloud system on the tropical island of la réunion. *Atmospheric Chemistry and Physics* 19, 10591–10618. doi:10.5194/acp-19-10591-2019.

Eleftheriadis, K., Colbeck, I., Housiadas, C., Lazaridis, M., Mihalopoulos,

- 891 N., Mitsakou, C., Smolík, J., Ždímal, V., 2006. Size distribution, compo-925
 892 sition and origin of the submicron aerosol in the marine boundary layer926
 893 during the eastern mediterranean “sub-aero” experiment. *Atmospheric*927
 894 *Environment* 40, 6245–6260. doi:10.1016/j.atmosenv.2006.03.059. 928
- 895 Foucart, B., Sellegri, K., Tulet, P., Rose, C., Metzger, J.M., Picard929
 896 D., 2018. High occurrence of new particle formation events at the930
 897 maïdo high-altitude observatory (2150 m), réunion (indian ocean)931
 898 *Atmospheric Chemistry and Physics* 18, 9243–9261. doi:10.5194/932
 899 acp-18-9243-2018. 933
- 900 Gantt, B., Meskhidze, N., 2013. The physical and chemical characteristic934
 901 of marine primary organic aerosol: a review. *Atmospheric chemistry*935
 902 *and physics* 13, 3979–3996. 936
- 903 Gao, R.S., Telg, H., McLaughlin, R.J., Ciciora, S.J., Watts, L.A., Richard937
 904 son, M.S., Schwarz, J.P., Perring, A.E., Thornberry, T.D., Rollins, A.W.938
 905 Markovic, M.Z., Bates, T.S., Johnson, J.E., Fahey, D.W., 2016. A light939
 906 weight, high-sensitivity particle spectrometer for pm2.5 aerosol mea-940
 907 surements. *Aerosol Science and Technology* 50, 88–99. doi:10.1080/941
 908 02786826.2015.1131809. 942
- 909 Guilpart, E., Vimeux, F., Evan, S., Brioude, J., Metzger, J.M., Barthe, C.943
 910 Risi, C., Cattani, O., 2017. The isotopic composition of near-surface wa-944
 911 ter vapor at the maïdo observatory (reunion island, southwestern indian945
 912 ocean) documents the controls of the humidity of the subtropical tro-946
 913 posphere. *Journal of Geophysical Research: Atmospheres* 122, 9628–947
 914 9650. doi:10.1002/2017JD026791. 948
- 915 Hamill, P., Giordano, M., Ward, C., Giles, D., Holben, B., 2016. A949
 916 aeronet-based aerosol classification using the mahalanobis distance. *At-950
 917 mospheric Environment* 140, 213–233. doi:10.1016/j.atmosenv.2016.951
 918 06.002. 952
- 919 Holben, B., Eck, T., Slutsker, I., Tanré, D., Buis, J., Setzer, A., Vermote953
 920 E., Reagan, J., Kaufman, Y., Nakajima, T., Lavenu, F., Jankowiak, I.954
 921 Smirnov, A., 1998. Aeronet—a federated instrument network and data955
 922 archive for aerosol characterization. *Remote Sensing of Environmen*956
 923 *t* 66, 1–16. doi:10.1016/S0034-4257(98)00031-5. 957
- 924 Inness, A., Baier, F., Benedetti, A., Bouarar, I., Chabrilat, S., Clark958
 925 H., Clerbaux, C., Coheur, P., Engelen, R.J., Errera, Q., Flemming,
 926 J., George, M., Granier, C., Hadji-Lazaro, J., Huijnen, V., Hurtmans,
 927 D., Jones, L., Kaiser, J.W., Kapsomenakis, J., Lefever, K., Leitão, J.,
 928 Razinger, M., Richter, A., Schultz, M.G., Simmons, A.J., Suttie, M.,
 929 Stein, O., Thépaut, J.N., Thouret, V., Vrekoussis, M., Zerefos, C.,
 930 2013. The MACC reanalysis: an 8 yr data set of atmospheric com-
 931 position. *Atmospheric Chemistry and Physics* 13, 4073–4109. doi:10.
 932 5194/acp-13-4073-2013.
- 933 Karol, Y., Tanré, D., Goloub, P., Vervaeerde, C., Balois, J.Y., Blarel, L.,
 934 Podvin, T., Mortier, A., Chaikovsky, A., 2013. Airborne sun photome-
 935 ter plasma: concept, measurements, comparison of aerosol extinction
 936 vertical profile with lidar. *Atmospheric Measurement Techniques* 6.
 937 doi:10.5194/amt-6-2383-2013.
- 938 Koren, I., Dagan, G., Altaratz, O., 2014. From aerosol-limited to invigora-
 939 tion of warm convective clouds. *Science* 344, 1143–1146. doi:10.1126/
 940 science.1252595.
- 941 Kusmierczyk-Michulec, J., de Leeuw, G., Gonzalez, C.R., 2002. Empir-
 942 ical relationships between aerosol mass concentrations and Ångström
 943 parameter. *Geophysical Research Letters* 29, 49–1–49–4. doi:10.1029/
 944 2001GL014128.
- 945 Lac, C., Chaboureaud, J.P., Masson, V., Pinty, J.P., Tulet, P., Escobar, J.,
 946 Leriche, M., Barthe, C., Aouizerats, B., Augros, C., Aumond, P., Au-
 947 guste, F., Bechtold, P., Berthet, S., Bielli, S., Bosseur, F., Caumont,
 948 O., Cohard, J.M., Colin, J., Couvreur, F., Cuxart, J., Delautier, G.,
 949 Dauhut, T., Ducrocq, V., Filippi, J.B., Gazen, D., Geoffroy, O., Gheusi,
 950 F., Honnert, R., Lafore, J.P., Lebeaupin Brossier, C., Libois, Q., Lunet,
 951 T., Mari, C., Maric, T., Mascart, P., Mogé, M., Molinié, G., Nuissier,
 952 O., Pantillon, F., Peyrillé, P., Pergaud, J., Perraud, E., Pianezze, J., Re-
 953 delsperger, J.L., Ricard, D., Richard, E., Riette, S., Rodier, Q., Schoet-
 954 ter, R., Seyfried, L., Stein, J., Suhre, K., Taufour, M., Thouron, O.,
 955 Turner, S., Verrelle, A., Vié, B., Visentin, F., Vionnet, V., Wautelet,
 956 P., 2018. Overview of the meso-nh model version 5.4 and its applica-
 957 tions. *Geoscientific Model Development* 11, 1929–1969. doi:10.5194/
 958 gmd-11-1929-2018.

- 959 Lafore, J.P., Stein, J., Asencio, N., Bougeault, P., Ducrocq, V., Duron
960 J., Fischer, C., Hérel, P., Mascart, P., Masson, V., Pinty, J.P., Re-
961 delsperger, J.L., Richard, E., Vilà-Guerau de Arellano, J., 1998. The
962 meso-nh atmospheric simulation system. part i: adiabatic formulation
963 and control simulations. *Annales Geophysicae* 16, 90–109. doi:10.1007/s00585-997-0090-6. 998
- 965 Lesouëf, D., Gheusi, F., Chazette, P., Delmas, R., Sanak, J., 2013. Low
966 tropospheric layers over reunion island in lidar-derived observations and
967 a high-resolution model. *Boundary-layer meteorology* 149, 425–453. doi:10.1007/s10546-013-9851-9. 1002
- 969 Louf, V., Pujol, O., Sauvageot, H., Riédi, J., 2015. Seasonal and diurnal wa-
970 ter vapour distribution in the sahelian area from microwave radiometric
971 profiling observations. *Quarterly Journal of the Royal Meteorological
972 Society* 141, 2643–2653. doi:10.1002/qj.2550. 1006
- 973 Luo, T., Yuan, R., Wang, Z., 2014. On factors controlling marine boundary
974 layer aerosol optical depth. *Journal of Geophysical Research: Atmos-
975 pheres* 119, 3321–3334. doi:10.1002/2013JD020936. 1009
- 976 Mallet, P.E., Pujol, O., Brioude, J., Evan, S., Jensen, A., 2018. Ma-
977 rine aerosol distribution and variability over the pristine southern indian
978 ocean. *Atmospheric Environment* 182, 17–30. doi:10.1016/j.atmosenv.2018.03.016. 1013
- 980 Morcrette, J.J., Boucher, O., Jones, L., Salmond, D., Bechtold, P., Bek-
981 jaars, A., Benedetti, A., Bonet, A., Kaiser, J.W., Razinger, M., Schulz
982 M., Serrar, S., Simmons, A.J., Sofiev, M., Suttie, M., Tompkins, A.M.,
983 Untch, A., 2009. Aerosol analysis and forecast in the european cen-
984 tre for medium-range weather forecasts integrated forecast system: For-
985 ward modeling. *Journal of Geophysical Research: Atmospheres* 114, 4019
986 doi:10.1029/2008JD011235. 1020
- 987 Myhre, G., Shindell, D., Bréon, F.M., Collins, W., Fuglestedt, J., Huang
988 J., Koch, D., Lamarque, J.F., Lee, D., Mendoza, B., Nakajima, T.,
989 Robock, A., Stephens, G., Takemura, T., Zhang, H., 2013. Anthro-
990 pogenic and Natural Radiative Forcing. *Cambridge University Press*
991 Cambridge, United Kingdom and New York, NY, USA. book section 8
992 p. 659–740. doi:10.1017/CBO9781107415324.018. 1026
- O’Dowd, C.D., de Leeuw, G., 2007. Marine aerosol production: a review of
the current knowledge. *Philosophical Transactions of the Royal Society
A: Mathematical, Physical and Engineering Sciences* 365, 1753–1774.
doi:10.1098/rsta.2007.2043.
- Pant, V., Deshpande, C., Kamra, A., 2009. The concentration and number
size distribution measurements of the marine boundary layer aerosols
over the indian ocean. *Atmospheric Research* 92, 381 – 393. doi:10.1016/j.atmosres.2008.12.004.
- Popovici, I., Goloub, P., Mortier, A., Podvin, T., Blarel, L., Loisel, R.,
Deroo, C., Victori, S., Torres, B., Unga, F., Choël, M., 2018. Un
système mobile pour l’étude de la distribution verticale des aérosols
dans l’atmosphère : description et premiers résultats. *Pollution atmo-
sphérique [Online]* 236. doi:10.4267/pollution-atmospherique.6510.
- Ramachandran, S., 2004. Spectral aerosol optical characteristics during the
northeast monsoon over the arabian sea and the tropical indian ocean:
1. aerosol optical depths and their variabilities. *Journal of Geophysical
Research: Atmospheres* 109. doi:10.1029/2003JD004476.
- Schuster, G.L., Dubovik, O., Holben, B.N., 2006. Angstrom exponent and
bimodal aerosol size distributions. *Journal of Geophysical Research -
Atmospheres* 111.
- Schwier, A., Sellegri, K., Mas, S., Charrière, B., Pey, J., Rose, C., Temime-
Roussel, B., Jaffrezo, J.L., Parin, D., Picard, D., Ribeiro, M., Roberts,
G., SEMPERE, R., Marchand, N., D’ANNA, B., 2017. Primary ma-
rine aerosol physical flux and chemical composition during a nutri-
ent enrichment experiment in mesocosms in the Mediterranean Sea.
Atmospheric Chemistry and Physics 17, 14645–14660. doi:10.5194/
acp-17-14645-2017.
- Seity, Y., Brousseau, P., Malardel, S., Hello, G., Bénard, P., Bouttier, F., Lac,
C., Masson, V., 2011. The arome-france convective-scale operational
model. *Monthly Weather Review* 139, 976–991.
- Stohl, A., Sodemann, H., Eckhardt, S., Frank, A., Seibert, P., Wotawa, G.,
2015. The lagrangian particle dispersion model flexpart version 8.2.
<https://www.flexpart.eu/wiki/FpDocumentation> .
- Verreyken, B., Amelynck, C., Schoon, N., Müller, J.F., Brioude, J., Kumps,

- 1027 N., Hermans, C., Metzger, J.M., Stavrakou, T., 2021. Measurement re-
1028 port: Source apportionment of volatile organic compounds at the remote
1029 high-altitude maïdo observatory. *Atmospheric Chemistry and Physics*
1030 *Discussions* 2021, 1–37. doi:10.5194/acp-2021-124.
- 1031 Verreyken, B., Brioude, J., Evan, S., 2019. Development of turbu-
1032 lent scheme in the flexpart-arome v1.2.1 lagrangian particle dispersion
1033 model. *Geoscientific Model Development* 12, 4245–4259. doi:10.5194/
1034 gmd-12-4245-2019.